NMR Experiments and Molecular Dynamics Simulations of the Segmental Dynamics of Polystyrene

Yiyong He, T. R. Lutz, and M. D. Ediger*

Department of Chemistry, University of Wisconsin−Madison, Madison, Wisconsin 53706

Chakravarthy Ayyagari, Dmitry Bedrov, and Grant D. Smith

Departments of Materials Science & Engineering and Chemical Engineering, University of Utah, Salt Lake City, Utah 84112

Received January 22, 2004; Revised Manuscript Received April 13, 2004

ABSTRACT: We have performed NMR spin−lattice relaxation experiments and molecular dynamics (MD) computer simulations on atactic polystyrene (a-PS). The segmental correlation times of three different molecular weight a-PS (M_n = 1600, 2100, 10 900 g/mol) were extracted from NMR by measuring the ^{2}H spin−lattice relaxation times (T_1) over a broad temperature range (390−510 K). MD simulations of an a-PS melt of molecular weight 2200 g/mol were carried out at 475, 500, and 535 K. Comparisons between experiments and simulations show that the MD simulations reproduce both the shape of the $P_2(t)$ orientation autocorrelation function and its temperature dependence, while the simulated segmental correlation times are slower than experimental results by a factor of 1.8. If the simulations are rescaled by this factor, they reproduce both the experimental T_1 values and the slight difference in dynamics between the backbone and side group of PS.

I. Introduction

The local dynamics of polymer melts, i.e., dynamics from the monomer length scale to that of the polymer statistical segment, are directly related to the conformation dynamics of the polymer and hence depend on the geometry, conformational energetics, and intermolecular interactions of a particular polymer. It is largely these local dynamics that distinguish one polymer from another and ultimately determine the dynamics of the polymer on all length scales. Currently, there are no theories that accurately describe polymer dynamics on length scales smaller than a statistical segment. Coordinated atomistic simulations and experimental studies of polymer melt dynamics can provide valuable insight into the microscopic origin of local polymer dynamics and help to develop theoretical models for these motions. Furthermore, such coordinated studies can provide guidance for new experiments and validate polymer force fields used in the simulations through comparisons of simulation predictions with experimental data.

A number of careful comparisons between experiments and simulations on local dynamics in polymer melts have already been reported.[1−18] Smith et al. have performed MD simulations of 1,4-polybutadiene and poly(ethylene oxide) and have made detailed comparison to NMR,[8,14] dielectric relaxation,[12] and neutron spin echo experiments.[5,7,15,16] Local dynamics in atactic polypropylene and polyisoprene melts were investigated by Theodorou and co-workers using a combination of MD simulations and several experimental techniques.[11,17] Smith et al. and Boyd and co-workers have combined NMR, dielectric relaxation, and MD simulation methods to gain insight into local dynamics of polyethylene.[1,18] In all cases, reasonable to excellent agreement between simulations and experiments was achieved. These studies clearly demonstrate the value and utility of carefully parametrized quantum chemistry based polymer potentials in reproducing experimentally measurable polymer dynamics as well as the insight that can be gained into polymer dynamics through combined experimental and simulation studies.

Almost all extensive comparisons between experiments and simulations for local dynamics in polymer melts have been performed on polymers with very simple chemical structures and low glass transitions temperatures. In this work, we compare the segmental dynamics of atactic polystyrene (a-PS) obtained from NMR experiments and MD simulations. Atactic PS is an important polymer with relatively high T_g. While MD simulations on the local translational and orientational mobility in a-PS have been reported by a few researchers,[19−21] these studies did not involve a close comparison with experimental measurements of polymer dynamics. The presence of phenyl rings in PS provides a significant complication in terms development of an accurate force field for use in MD simulations. The force field must be able to describe not only the conformational energetics (relative energies of low-energy conformers and the barriers between them) but also the rotational energetics of the phenyl rings and the interaction between phenyl rings. Based primarily upon quantum chemistry studies of phenyl ring interactions[22] and 2,4-diphenylpentane, we have parametrized a quantum chemistry based potential[23] that will be utilized, and tested, in this work.

In this study, ^{2}H T_1 was measured for three atactic polystyrene samples with different molecular weights (M_n = 1600, 2100, 10 900 g/mol). A wide range of temperatures (390−510 K) were investigated at three magnetic fields. The segmental correlation times $\tau_{seg,c}$ were extracted by fitting T_1 data to the modified Kohlrausch−Williams−Watts (mKWW) autocorrelation function and the Vogel−Tammann−Fulcher (VTF) equation. The MD simulations were performed on an a-PS

* Corresponding author: e-mail ediger@chem.wisc.edu.

10.1021/ma049843r CCC: $27.50
Published on Web 05/26/2004

Table 1. Characterization of PS Samples

samples	M_n (g/mol)	M_w/M_n	T_g (K)
d_3PS-1	1600	1.28	319
d_8PS-2	2100	1.10	331
d_8PS-11	10900	1.05	367

melt (M_n = 2200 g/mol) at 475, 500, and 535 K. Comparisons between experiments and simulations were made in terms of the $P_2(t)$ autocorrelation function for C−^{2}H vectors, segmental correlation times, and T_1 values.

II. Experiments and Simulation Methodology

Materials and Characterization. Characterization information for the three deuterated a-PS samples is listed in Table 1. Perdeuterated polystyrenes, d_8PS-2 (M_n = 2100 g/mol) and d_8PS-11 (M_n = 10 900 g/mol), were purchased from Polymer Source, Inc. Backbone deuterated polystyrene d_3PS-1 (M_n = 1600 g/mol) was synthesized by Dr. Marinos Pitsikalis. The synthetic procedure was very similar to that used in ref 24 and will be described in a future publication. M_n and M_w/M_n were determined by size exclusion chromatography (SEC). Differential scanning calorimetry (DSC) measurements were carried out on a Netzsch 200 DSC. T_g is determined as the midpoint of the transition during heating with a scan rate of 10 K/min after cooling the sample at the same rate from well above T_g.

NMR Measurements. All samples were prepared by loading 0.4 g of granular PS into 5 mm NMR tubes and sealing them under vacuum. The tubes were then placed in an oven at 150 °C for half an hour to allow the samples to flow to the bottom of the NMR tubes.

^{2}H T_1 was measured by the standard inversion−recovery ($\pi-\tau-\pi/2$) pulse sequence, waiting more than 10 times T_1 between the acquisition and the next pulse. The number of scans used for signal averaging ranges from 8 to 128, depending on the temperature. An average T_1 value, based on at least three runs, is used for analysis at each temperature. The uncertainty in T_1 is ±3%. All measurements were performed on a Varian Inova-500 NMR spectrometer (76.8 MHz) and a Bruker DMX-300 NMR spectrometer (46.1 and 15.3 MHz). Spectra were processed with line broadening equal to one-tenth of the full width at half-height of the spectra, followed by fitting the peak intensities to a three-parameter exponential function. Temperature was controlled to ±0.5 K and calibrated to within an uncertainty of ±2 K using a combination of an ethylene glycol thermometer[25] and melting point standards. Several tests[26] were performed to ensure that no detectable degradation took place during experiments.

NMR Relaxation Mechanism and Correlation Function. For ^{2}H nuclei, spin−lattice relaxation is dominated by electric quadrupole coupling. The relationship between the spin relaxation time and the reorientation of a C−^{2}H bond is given in the next three equations.[27−30]

$$\frac{1}{T_1} = \frac{3}{10}\pi^2\left(\frac{e^2qQ}{h}\right)^2 [J(\omega_D) + 4J(2\omega_D)] \quad (1)$$

Here $\omega_D/2\pi$ is the Larmor frequency of deuterium. The quadrupole coupling constant e^2qQ/h was taken as 172 and 190 kHz for the backbone and phenyl ring deuterons, respectively.[30−32] $J(\omega)$ is the spectral density function:

$$J(\omega) = {}^1/_2\int_{-\infty}^{\infty} P_2(t)\exp(-i\omega t)\,dt \quad (2)$$

Here $P_2(t)$ is the orientation autocorrelation function which describes the reorientation of the internuclear vector (C−^{2}H in the experiments and C−H in the simulations):

$$P_2(t) = \frac{3}{2}\langle\cos^2\theta(t)\rangle - \frac{1}{2} \quad (3)$$

Here $\theta(t)$ is the angle of a C−^{2}H or C−H bond at time t relative to its original position. The brackets denote the ensemble average over a collection of nuclei.

In previous studies,[33−35] the mKWW equation was shown to give an excellent representation of the autocorrelation function $P_2(t)$:

$$P_2(t) = a_{lib}\exp\left(-\frac{t}{\tau_{lib}}\right) + (1 - a_{lib})\exp\left[-\left(\frac{t}{\tau_{seg}}\right)^{\beta}\right] \quad (4)$$

Here a_{lib} and τ_{lib} characterize the amplitude and relaxation time for librational motion. τ_{lib} was fixed at 1 ps since the fitting procedure is not sensitive to the precise value of this parameter. τ_{seg} and β describe a characteristic segmental relaxation time as well as its distribution. We assume a VTF temperature dependence[36,37] for τ_{seg}

$$\log\left(\frac{\tau_{seg}}{\tau_\infty}\right) = \frac{B}{T - T_0} \quad (5)$$

where τ_∞, B, and T_0 are constants for a particular sample. The segmental correlation time $\tau_{seg,c}$ is defined as the integral of the segmental portion of the correlation function:

$$\tau_{seg,c} = \frac{\tau_{seg}}{\beta}\Gamma\left(\frac{1}{\beta}\right) \quad (6)$$

Simulation Methodology. MD simulations were performed on a melt of 16 a-PS chains, each consisting of 21 repeat units (M = 2200 g/mol) at 475, 500, and 535 K employing an explicit atom force field. Initially, the force field has been parametrized to reproduce conformational energies of isopropylbenzene[23] and 2,4-diphenylpentane[23] as well as binding energies of benzene dimer[22] obtained from quantum chemistry calculations. Subsequent simulations of liquid-phase racemic and meso 2,4-diphenylpentane revealed that conformational populations of 2,4-diphenylpentane are in some disagreement with NMR conformational analysis for the same compound.[38] We therefore slightly modified torsional parameters for the backbone dihedrals in the force field from ref 23 to improve agreement with experimental conformational populations in the liquid phase. The complete description of the force field used in this work as well as in our previous simulations of a polystyrene melt[39] is given in Table 1 of the Supporting Information.

Initially the chains were placed on a low-density lattice. Stochastic dynamics[40] were performed at high temperatures, and subsequently the system was cooled to liquid densities at 475 K over a period of 0.5 ns. Simulations were performed for about 0.5 ns in an isobaric−isothermal ensemble to obtain the equilibrium density at each temperature. The equilibrium densities obtained for the a-PS melt were 0.98 g/cm^3 (475 K), 0.969 g/cm^3 (500 K), and 0.958 g/cm^3 (535 K), which are within 1.0−1.5% from experimental values.[41] Bond lengths were constrained using the SHAKE algorithm[42] for all simulations. A cutoff radius of 9 Å for nonbonded interactions was used, and electrostatic interactions were treated using the particle-mesh Ewald (PME) algorithm.[43] Production runs in the NVT ensemble have been performed over 45 ns with an integration time step of 1 fs, using the Nose-Hoover thermostat and explicit reversible integrators described elsewhere.[44] The calculated autocorrelation functions decay to less than 0.003 at long times.

III. Results

NMR Spin−lattice Relaxation Times. ^{2}H T_1 values for the three a-PS samples measured at 76.8, 46.1, and 15.3 MHz are presented in Figure 1 as symbols. The T_1 minimum moves to higher temperatures as the molecular weight of a-PS increases. Since the T_1 minimum approximately indicates the temperature at which the segmental dynamics occur on a 1 ns time scale, this

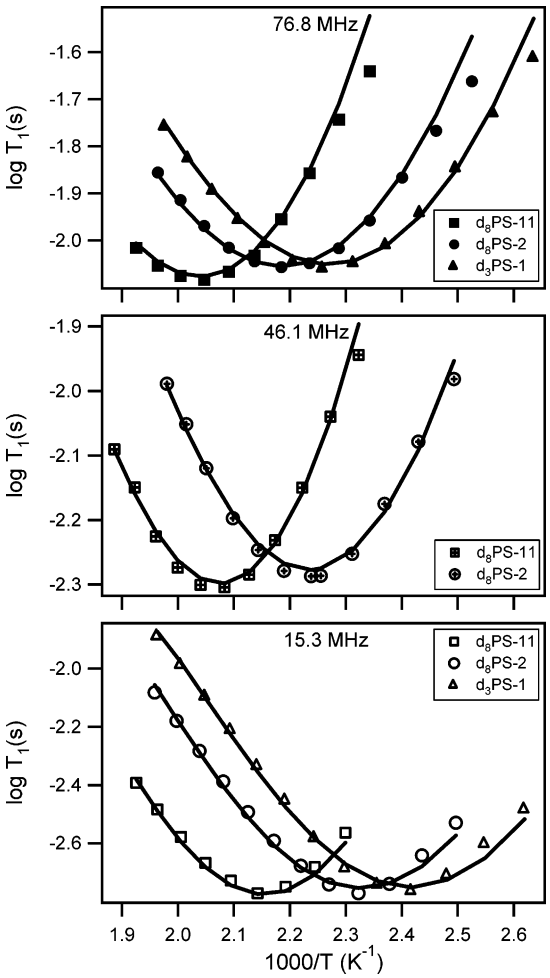

Figure 1. ^{2}H NMR spin−lattice relaxation time measurements for three PS samples at 76.8, 46.1, and 15.3 MHz, plotted as log base 10. For the perdeuterated PS (d_8), the rate averaged T_1 values for backbone and phenyl ring deuterons are presented. Solid curves are fits using the mKWW autocorrelation function and VTF equation. The fit parameters are listed in Table 3.

Table 2. Horizontal and Vertical Shifts Needed To Superpose the Experimental Data of d_3PS-1 and d_8PS-2 onto d_8PS-11

samples	$\Delta\log(T_1)$ (s)	ΔT (K)	ΔT_0 (K)[a]	ΔT_g (K)
d_3PS-1	−0.02	50	48	48
d_8PS-2	−0.02	35	39	36

[a] From fits in Table 3.

indicates that the segmental dynamics of a-PS become slower with increasing molecular weight. Qualitatively, such a relationship between the segmental dynamics and molecular weight is expected in this molecular weight regime. For perdeuterated samples d_8PS-2 and d_8PS-11, substantial overlaps were observed at low temperatures between the backbone and phenyl ring deuterium resonance peaks. Since the two kinds of deuterons have similar T_1 values and very similar temperature dependences (see the inset in Figure 8), we averaged the T_1 values over the eight deuterons at all temperatures and used these rate-averaged T_1 values in our analysis of these two samples. The experimental T_1 data for the backbone and phenyl ring deuterons and the rate-average calculation can be found in Table 2 of the Supporting Information.

Superposition of the NMR Data. A model-independent way of examining the molecular weight dependence of segmental dynamics is to directly superpose the experimental data using temperature shifts.[45] As shown in Figure 2, we found that temperature shifts (not shifts in terms of 1000/T) produced reasonable master curves for the three PS samples. These master curves indicate that the different molecular weight samples have segmental dynamics with very similar temperature dependences and that the shape of the orientation autocorrelation function is essentially the same for these three samples. (Similar conclusions, for PS samples near T_g, were obtained by Santangelo and Roland.[46]) Very small vertical shifts were also needed to superpose the T_1 data (see Table 2). The superposition is nearly perfect, and it is adequate to provide a model-independent check on the fitting results obtained below. A strong indication that these shifts are meaningful is the fact that the same temperature and vertical shifts sufficed to superpose the T_1 data at three different fields. As shown by the shift parameters in Table 2, the temperature shifts for superposition (ΔT) closely track the T_g differences (ΔT_g).

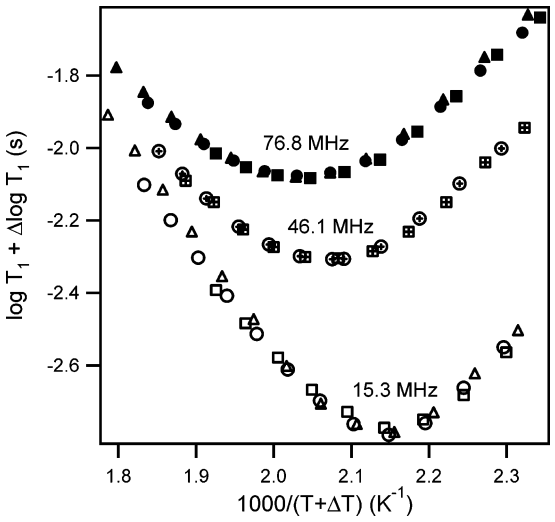

Figure 2. Superposition of the T_1 data (same symbol codes as in Figure 1). A single temperature and vertical shift suffice to superpose the data at 76.8, 46.1, and 15.3 MHz simultaneously for each sample. Shift parameters are listed in Table 2.

Segmental Correlation Times from NMR Experiments. Since it was found in previous studies[33−35] that the mKWW function (eq 4) provides excellent fits to the NMR T_1 (and NOE) data, we employed it here in combination with the assumption of a VTF temperature dependence for the segmental relaxation times (eq 5). Fitting was performed on the experimental data sets (all frequencies simultaneously) for each sample using eqs 1−5. The NMR experiments do not directly measure the $P_2(t)$ orientation autocorrelation function. To obtain $P_2(t)$, we make an initial guess about the fit parameters, calculate the resulting T_1 values, and then optimize the parameters to provide the best fit to the T_1 data. There are five unknown parameters in this procedure: a_{lib}, β, τ_∞, B, and T_0. Because of the relatively small range of correlation times probed by NMR measurements, B and T_0 are highly correlated with each other, and some constraint is desirable. In our fitting, we constrained the extrapolated segmental dynamics at the DSC T_g to be 1 s. The fit parameters are summarized in Table 3. As a check, we also fit the data without any constraint on the five parameters (parameters not reported here). The two methods yield essentially the same $\tau_{seg,c}$ values,

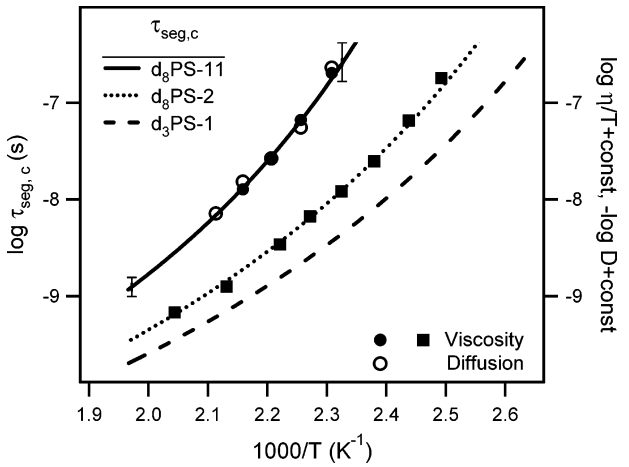

Figure 3. Segmental correlation times from NMR experiments and their relationship to the terminal dynamics extracted from viscosity and diffusion measurements (refs 50 and 51). The correlation times of the three PS samples were calculated using the fit parameters in Table 3 and are shown as lines. Representative error bars are shown and reflect the uncertainty associated with the fitting procedure. Arbitrary vertical shifts were made to the viscosity and diffusion data in order to compare the temperature dependence.

Table 3. Best Fit Parameters (mKWW and VTF Equations) for the Segmental Dynamics of PS Samples from NMR Measurements

	samples		
parameters	d_3PS-1	d_8PS-2	d_8PS-11
β	0.44	0.44	0.44
τ_∞ (ps)	0.12	0.10	0.14
T_0 (K)	265	274	313
B (K)	686	728	681
a_{lib}	0.14	0.23	0.19

never differing by more than 0.15 decades in the temperature range of our measurements. The experimental uncertainty in $\tau_{seg,c}$ is shown in Figure 3 by the representative error bars. Because of the correlations between B and T_0, and between a_{lib} and β, these four parameters have substantial uncertainty: B is accurate within ±80 K, T_0 is accurate within ±12 K, and both a_{lib} and β have an uncertainty of ±0.07. As shown by the solid lines in Figure 1, the parameters in Table 3 produce excellent fits to the experimental T_1 data, except for the points at the lowest temperature.

The segmental correlation times were calculated from the fit parameters in Table 3 using eq 6. The resulting curves are plotted in Figure 3. The shapes of the correlation time curves are identical for the three PS samples over the temperature range of the NMR study. If we move the three curves by the same amount as ΔT (temperature shifts needed to superpose the experimental data) in Table 2, an excellent master curve is achieved (not shown here). This is another strong indication of the robustness of the fitting procedure. The uncertainty in the reported correlation times, as reflected by different fitting procedures, is shown by the representative error bars in Figure 3.

At temperatures far above T_g, it is expected that segmental and terminal relaxation processes in a typical polymer melt will have the same temperature dependence.[47] (Very near T_g, different temperature dependences have been observed for a-PS and other polymers.[48,49]) Recently self-diffusion and viscosity measurements on a-PS samples of 2000 and 11 000 g/mol

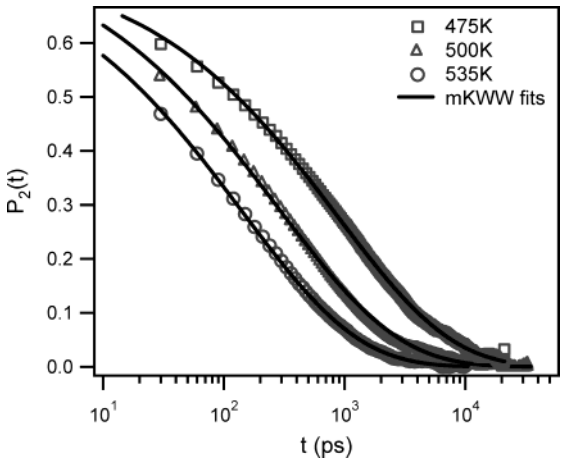

Figure 4. $P_2(t)$ autocorrelation functions from MD simulations for d_8PS-2 at 475, 500, and 535 K. The weight-average of the correlation functions for the backbone and phenyl ring C−H vectors are shown. Solid curves are the mKWW fits.

Table 4. Best Fit Parameters (mKWW Equation) for the $P_2(t)$ Autocorrelation Functions of d_8PS-2 from MD Simulations

		parameters		
temp (K)	C−^{2}H vector	β	τ_{seg} (ns)	a_{lib}
475	backbone	0.45	0.93	0.20
	phenyl ring	0.47	0.85	0.28
	average	0.46	0.88	0.24
500	backbone	0.45	0.35	0.20
	phenyl ring	0.43	0.24	0.20
	average	0.43	0.28	0.20
535	backbone	0.47	0.17	0.21
	phenyl ring	0.44	0.12	0.22
	average	0.45	0.14	0.22

have been reported.[50,51] Comparisons between these measurements of terminal dynamics and our segmental dynamics results are shown in Figure 3. Arbitrary vertical shifts have been made to the diffusion and viscosity data in order to compare the temperature dependence unambiguously. As can be clearly seen, the terminal dynamics perfectly track the temperature dependence of the segmental dynamics in the temperature range of NMR study (above T_g + 60 K).

Autocorrelation Functions from MD Simulations. The simulated melt of a-PS chains each with 21 repeat units matches the molecular weight of the d_8PS-2 sample. The C−H vector autocorrelation functions from the simulations will be compared to the C−^{2}H vector information from the experiments; i.e., we assume no influence of deuteration on the dynamics. The C−H vector $P_2(t)$ autocorrelation functions illustrated in Figure 4 were determined from the simulation trajectories using eq 3. The simulation trajectories have been analyzed for the backbone and phenyl ring C−H vectors of PS. To be consistent with the NMR measurements, the weighted average autocorrelation functions over the eight C−H vectors are presented in Figure 4. A nonexponential decay is observed at all three temperatures. The simulation results were successfully fit by the mKWW function (eq 4) with the fit parameters given in Table 4. Table 4 also shows that the backbone and side group have similar shapes of $P_2(t)$ autocorrelation function, with the side group having slightly faster relaxation times than the backbone. The β and a_{lib} values reported in Table 4 are close to the fit parameters

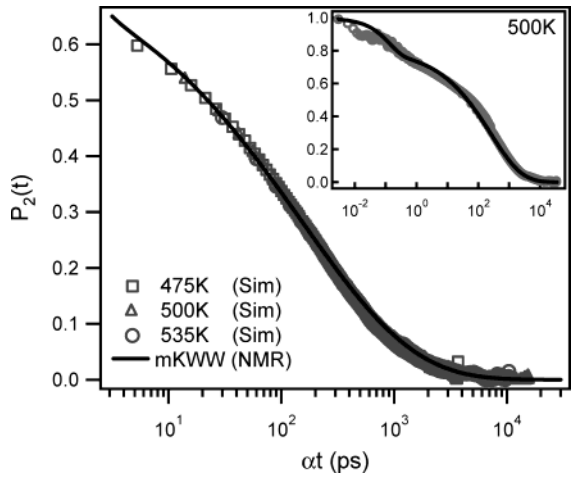

Figure 5. Superposition of the simulated $P_2(t)$ curves shown in Figure 4 (using $\alpha = 1$, 0.48, and 0.17 for simulations at 535, 500, and 475 K curves, respectively). The solid line is the mKWW autocorrelation function for d_8PS-2 obtained from fits to the NMR data, shifted in time to overlap the simulation curves. The inset shows the simulated $P_2(t)$ curve at 500 K over a larger time window. The solid line in the inset is a mKWW fit with $\beta = 0.43$, $\tau_{seg} = 250$ ps, $a_{lib} = 0.195$, and $\tau_{lib} = 0.13$ ps.

for d_8PS-2 from the NMR data (see Table 3). We will further address this issue below.

IV. Discussion

The primary goal of this coordinated simulation and experimental study of a-PS melts is to investigate the ability of the quantum chemistry based potential to reproduce the local dynamics in a high-T_g polymer with complex intramolecular interactions. A second goal is to test the procedures used to extract the information about dynamics from the NMR measurements. For these purposes we make an extensive comparison of the NMR experimental measurements, fitting results, and molecular dynamics simulations for d_8PS-2.

Shape of the Orientation Autocorrelation Function. Figure 5 presents a master curve of the simulated $P_2(t)$ autocorrelation functions at 475, 500, and 535 K, obtained by shifting the curves from Figure 4 along the logarithmic time axis. The superposition is excellent, strongly supporting the assumption (see eq 4) of temperature independence for the autocorrelation function shape (i.e., a_{lib} and β are constant) at temperatures well above T_g. Since the NMR experiment does not directly measure the autocorrelation function, we need to extract it from the experimental data through the use of a model. In Figure 1, we showed that fits using the mKWW function provide an excellent description of the NMR data. Thus, the mKWW equation with the fit parameters for d_8PS-2 in Table 3 should be a good representation of the actual autocorrelation function. This is plotted in Figure 5 as a solid line. The agreement between the simulation and experiment is excellent.

It is interesting to examine the shape of the orientation autocorrelation function in a much wider time window using results from the MD simulations. The inset of Figure 5 shows the simulated $P_2(t)$ curve at 500 K extending to times as short as 0.003 ps. The solid line is a fit to the mKWW function. The mKWW equation well describes the entire simulated $P_2(t)$ curve, except for some deviation at times less than 1 ps. The fit parameters β, τ_{seg}, and a_{lib} are very similar to those

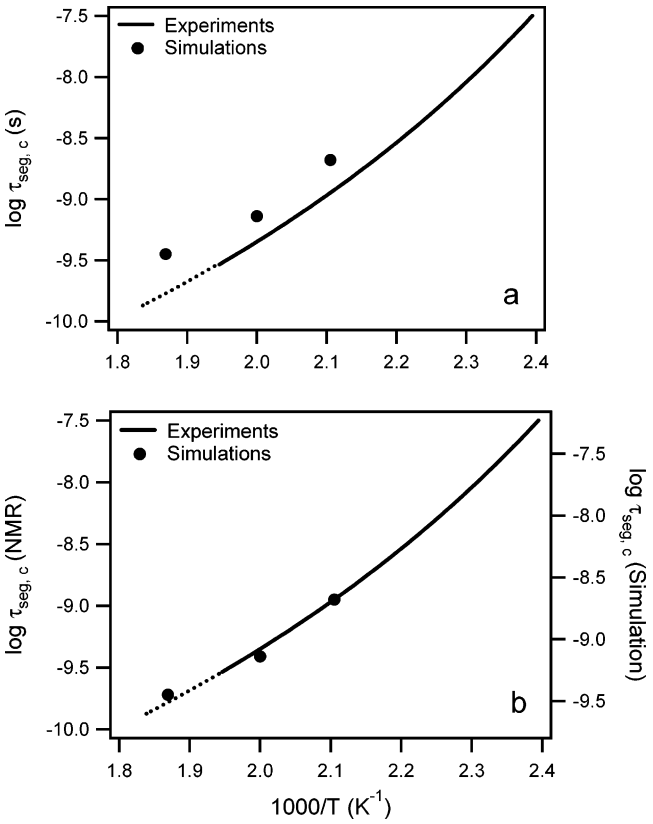

Figure 6. Segmental correlation times of d_8PS-2 from NMR experiments (solid lines) and MD simulations (points): (a) direct comparison; (b) rescaled comparison by reducing the simulated relaxation time by a factor of 1.8. The dashed lines represent extrapolations of the NMR results based on the fit parameters in Table 3.

obtained from the fit to the simulation autocorrelation function curve at long times (Table 4); the fit parameter τ_{lib} is equal to 0.13 ps in the inset to Figure 5 while our fitting of the NMR data used $\tau_{lib} = 1$ ps. The deviations shown at short times in the inset and the smaller value of τ_{lib} obtained from fitting the simulation results have no impact on the quantitative comparison between the simulations and the NMR experiments. As shown in eq 1, T_1 depends on frequency components in the autocorrelation function in the frequency range from 100 to 1000 MHz. The very short time discrepancies described in this paragraph have essentially no impact on the spectral density function in the relevant frequency range; for example, changing τ_{lib} from 1 to 0.13 ps changes predictions for T_1 by less than 1%. The subpicosecond dynamics correspond to the rapid librational motion of C−H vectors and not to transitions between conformational states.

Segmental Correlation Times. Next we compare the absolute segmental relaxation times and their temperature dependences. Figure 6 shows the experimental correlation times as a solid line; the dashed lines represent an extrapolation to higher temperatures. The simulated correlation times can be calculated from eq 6 using the average fit parameters in Table 4 and are plotted in the same figure as circles. Figure 6a shows that the segmental dynamics of the simulated a-PS chains are systematically too slow. In Figure 6b, the two sets of data are shifted by a factor of 1.8, showing that they have the same temperature dependence.

One way of accounting for the too slow segmental dynamics observed in the simulations is to assume that

the force field does not perfectly reproduce the conformational energy barriers for a-PS. We would expect reduction of the barriers between important conformers of a-PS by 0.5 kcal/mol to result in a speed-up of segmental dynamics by almost a factor of 2 at the temperatures investigated here. Uncertainties on the order of 0.5 kcal/mol in the conformational energy barriers are anticipated due to uncertainties in the conformational energetics obtained for model compounds (2,4-diphenylpentane) from quantum chemistry, which result from errors introduced by basis set limitations and treatment of electron correlation. Additionally, the simple form of the classical force field used in the simulation does not perfectly match the conformational energetics of the model compound obtained from quantum chemistry. Considering the complexity of a-PS and the intrinsic difficulties involved in high-level quantum chemistry studies of PS model compounds, we consider the ability of the force field (without empirical adjustment) to reproduce local dynamics in a-PS melts as demonstrated here to be more than satisfactory.

Spin−Lattice Relaxation Times. In this section we compare the results from the MD simulation and NMR experiment in an alternate way: we fit the simulated $P_2(t)$ autocorrelation functions at each temperature to an analytical function, then Fourier transform to get the spectral density function $J(\omega)$ (eq 2), and finally calculate the T_1 values for the simulated chains (eq 1). There is a reason for making this additional comparison. In the above discussion the autocorrelation function and segmental correlation times from NMR experiments were extracted using a fitting procedure which is based on a number of assumptions. It is desirable to have a model-free comparison between the simulations and the experimental data.

The T_1 values obtained from the simulations in this manner are compared with the experimental data in Figure 7a. Since we already know from Figure 6 that the simulated PS dynamics are slower than experimental results, some disagreement is expected. Values from the simulations are systematically smaller than those observed experimentally at the left side of the T_1 minimum, consistent with the slower dynamics. We rescale the simulated relaxation times by 0.56 (= 1/1.8) and make the comparison again in Figure 7b, achieving nearly perfect agreement. This comparison validates the use of the mKWW function to extract the orientational dynamics from the experimental T_1 data.

Difference in Dynamics for Backbone and Phenyl Ring. Both NMR experiments and MD simulations show that the backbone and phenyl ring C−H vectors in a-PS have slightly different dynamics. In the NMR experiments, the deuterium resonance signals for the backbone and phenyl ring deuterons can only be well resolved at 76.8 MHz and also at high temperatures (as shown by the inset in Figure 8). We fit the points at the left side of T_1 minimum using the same procedure described in the previous section. The resulting segmental correlation times for the backbone and side-group C−H vectors in a-PS are presented in Figure 8. The simulation correlation times, calculated from Table 4 and shifted by 1/1.8, are plotted in the same figure. Clearly, the rescaled MD simulations well reproduce the slight difference in dynamics between backbone and phenyl ring C−H vectors in a-PS. This agreement provides an additional check on some aspects of the force field employed here, e.g., the relative height of the

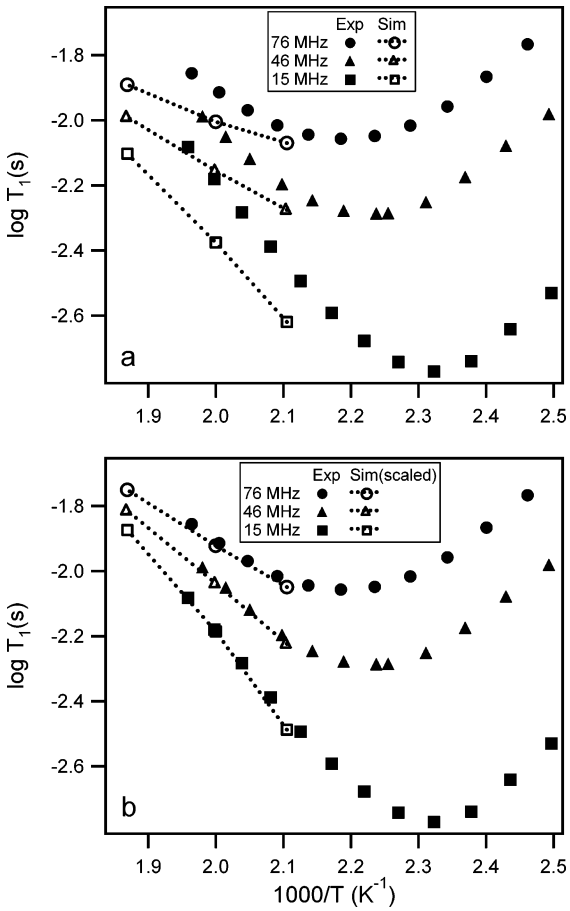

Figure 7. Rate-averaged ^{2}H spin−lattice relaxation times T_1 for all C−^{2}H vectors in d_8PS-2 at 76.8, 46.1, and 15.3 MHz, as measured from NMR experiments and predicted from MD simulations: (a) direct comparison; (b) reducing simulation time by a factor of 1.8. The dotted lines guide the eye.

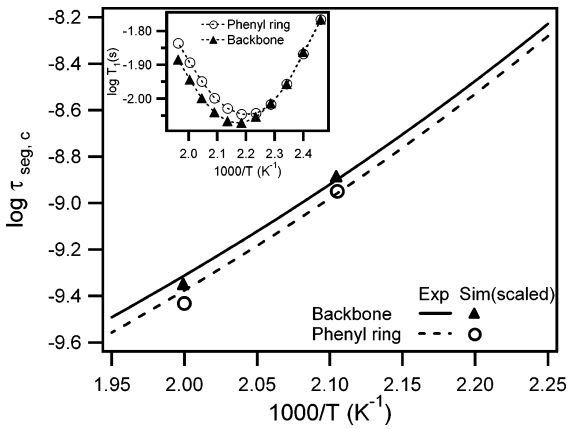

Figure 8. Segmental correlation times for backbone and phenyl ring C−H vectors of 2100 g/mol a-PS from NMR experiments and MD simulations. The simulated correlation times are scaled by a factor of 1/1.8. The NMR fit parameters for the backbone deuterons are $\tau_\infty = 0.075$ ps, $B = 774$ K, $T_0 = 271$ K, $\beta = 0.43$ and for the phenyl ring deuterons are $\tau_\infty = 0.055$ ps, $B = 782$ K, $T_0 = 271$ K, $\beta = 0.42$. The inset shows the experimental ^{2}H NMR spin−lattice relaxation times for d_8PS-2 at 76.8 MHz; the dotted lines guide the eye.

energy barriers for the backbone and side group. Because of a limited number of data points, the correlation times from the NMR experiments in Figure 8 are less reliable than the fits discussed above. Nevertheless, their average still falls on the dotted line (d_8PS-2) in Figure 3 within the reported experimental uncertainty.

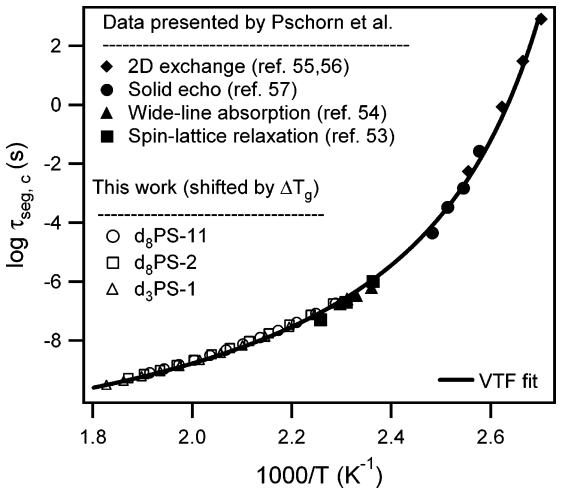

Figure 9. Mean segmental correlation times of PS obtained from various NMR experiments. The open symbols were calculated using the fit parameters in Table 3 and horizontally shifted by ΔT_g, taking $T_g = 373$ K for high molecular weight PS. The solid line is a VTF fit curve over the whole temperature range explored with parameters $\tau_\infty = 0.87$ ps, $B = 542$ K, and $T_0 = 334.7$ K.

Comparison to NMR Experiments at Lower Temperatures. Pschorn et al. published a paper in 1991 which compiled a variety of NMR measurements on the segmental dynamics of polystyrene over the temperature range from T_g to $T_g + 70$ K.[52] Our experiments allow us to expand the temperature range of this compilation up to $T_g + 180$ K. Figure 9 shows the combined results from 2D exchange, solid echo, wide-line absorption, and spin−lattice relaxation measurements at low and high temperatures. The solid points are all taken from Figure 3 in ref 52, with their original sources of refs 53−57. The open symbols were calculated using the fit parameters in Table 3 and horizontally shifted by ΔT_g, taking $T_g = 373$ K for high molecular weight PS (solid points).[52]

Our new measurements smoothly extend the previous measurements, and a single VTF fit reasonably describes the combined data set. The slight mismatch at $1000/T \approx 2.25$ is at the same level as experimental error.

V. Conclusions

We have investigated the segmental dynamics of three atactic polystyrene samples with different molecular weights by NMR. ^{2}H T_1 measurements at three magnetic fields over a broad temperature range were performed to extract the $P_2(t)$ orientation autocorrelation function and the segmental correlation times $\tau_{seg,c}$. For one of the samples ($M_n = 2100$ g/mol), rigorous comparisons to MD simulations were made in terms of $P_2(t)$, $\tau_{seg,c}$, and T_1 values.

There are two major findings of this study: (1) The NMR experiments and MD simulations for a low molecular weight a-PS melt are in very good agreement. The simulations correctly predict the shape of $P_2(t)$ autocorrelation function and its temperature dependence. The simulated segmental correlation times are slower than the experimental results by a factor of 1.8, a difference that can be accounted for by uncertainties in the conformational energy barriers in the quantum chemistry based force field for a-PS. After rescaling all the simulated relaxation times by a single factor, the simulations reproduce the rate average T_1 values and the slight difference in dynamics between the backbone and side group of polystyrene. (2) The segmental dynamics of polystyrene chains in this low molecular weight range, at temperatures well above T_g, are identical at the same value of $T - T_g$. Over the temperature range of this NMR study, the segmental and terminal dynamics have essentially the same temperature dependence.

Acknowledgment. This work is supported by the National Science Foundation (DMR-0099849 and DMR-0355470) and supported in part by a fellowship from Merck Research Laboratories (Y.H.). We thank Dr. Charles Fry for the help with the instrument and Prof. Paul Nealey for the use of the DSC. Some measurements were performed at the Instrument Center of the Department of Chemistry, University of Wisconsin−Madison, supported by NSF CHE-9629688. The fitting work was done at the computer center of the Department of Chemistry, University of Wisconsin−Madison, supported by NSF CHE-0091916. Simulations were performed at University of Utah and funded by the University of Utah Center for the Simulation of Accidental Fires and Explosions (C-SAFE), funded by the Department of Energy, Lawrence Livermore National Laboratory, under Subcontract B524196.

Supporting Information Available: Table 1 listing the complete parameter set of the force field used in this work and Table 2 showing the experimental ^{2}H T_1 data for the three a-PS samples measured at 76.8, 46.1, and 15.3 MHz. This material is available free of charge via the Internet at http://pubs.acs.org.

References and Notes

(1) Smith, G. D.; Yoon, D. Y.; Zhu, W.; Ediger, M. D. *Macromolecules* **1994**, *27*, 5563−5569.
(2) Paul, W.; Yoon, D. Y.; Smith, G. D. *J. Chem. Phys.* **1995**, *103*, 1702−1709.
(3) Smith, G. D.; Paul, W.; Yoon, D. Y.; Zirkel, A.; Hendricks, J.; Richter, D.; Schober, H. *J. Chem. Phys.* **1997**, *107*, 4751−4755.
(4) Paul, W.; Smith, G. D.; Yoon, D. Y. *Macromolecules* **1997**, *30*, 7772−7780.
(5) Paul, W.; Smith, G. D.; Yoon, D. Y.; Farago, B.; Rathgeber, S.; Zirkel, A.; Willner, L.; Richter, D. *Phys. Rev. Lett.* **1998**, *80*, 2346−2349.
(6) Smith, G. D.; Yoon, D. Y.; Wade, C. G.; O'Leary, D.; Chen, A.; Jaffe, R. L. *J. Chem. Phys.* **1997**, *106*, 3798−3805.
(7) Smith, G. D.; Paul, W.; Monkenbusch, M.; Willner, L.; Richter, D.; Qiu, X. H.; Ediger, M. D. *Macromolecules* **1999**, *32*, 8857−8865.
(8) Smith, G. D.; Borodin, O.; Bedrov, D.; Paul, W.; Qiu, X. H.; Ediger, M. D. *Macromolecules* **2001**, *34*, 5192−5199.
(9) Moe, N. E.; Ediger, M. D. *Polymer* **1996**, *37*, 1787−1795.
(10) Harmandaris, V. A.; Doxastakis, M.; Mavrantzas, V. G.; Theodorou, D. N. *J. Chem. Phys.* **2002**, *116*, 436−446.
(11) Doxastakis, M.; Theodorou, D. N.; Fytas, G.; Kremer, F.; Faller, R.; Muller-Plathe, F. *J. Chem. Phys.* **2003**, *119*, 6883−6894.
(12) Smith, G. D.; Borodin, O.; Paul, W. *J. Chem. Phys.* **2002**, *117*, 10350−10359.
(13) Borodin, O.; Douglas, R.; Smith, G. D.; Trouw, F.; Petrucci, S. *J. Phys. Chem. B* **2003**, *107*, 6813−6823.
(14) Smith, G. D.; Borodin, O.; Pekny, M.; Annis, B.; Londono, D.; Jaffe, R. L. *Spectrochim. Acta, Part A* **1997**, *53*, 1273−1283.
(15) Smith, G. D.; Paul, W.; Monkenbusch, M.; Richter, D. *J. Chem. Phys.* **2001**, *114*, 4285−4288.
(16) Saboungi, M.-L.; Price, D. L.; Mao, G.; Fernandez-Perea, R.; Borodin, O.; Smith, G. D.; Armand, M.; Howells, W. S. *Solid State Ionics* **2002**, *147*, 225−236.
(17) Ahumada, O.; Theodorou, D. N.; Triolo, A.; Arrighi, V.; Karatasos, C.; Ryckaert, J.-P. *Macromolecules* **2002**, *35*, 7110−7124.
(18) Jin, Y.; Boyd, R. H. *J. Chem. Phys.* **1998**, *108*, 9912−9923.

(19) Roe, R. J. *J. Non-Cryst. Solids* **1998**, *235*−*237*, 308−313.
(20) Lyulin, A. V.; Michels, M. A. J. *Macromolecules* **2002**, *35*, 1463−1472.
(21) Lyulin, A. V.; Balabaev, N. K.; Michels, M. A. J. *Macromolecules* **2002**, *35*, 9595−9604.
(22) Smith, G. D.; Jaffe, R. L. *J. Phys. Chem.* **1996**, *100*, 9624−9630.
(23) Smith, G. D.; Ayyagari, C.; Jaffe, R. L.; Pekny, M.; Bernarbo, A. *J. Phys. Chem. A* **1998**, *102*, 4694−4702.
(24) Min, B.; Qiu, X. H.; Ediger, M. D.; Pitsikalis, M.; Hadjichristidis, N. *Macromolecules* **2001**, *34*, 4466−4475.
(25) Kaplan, M. L.; Bovey, F. A.; Cheng, H. N. *Anal. Chem.* **1975**, *47*, 1703−1705.
(26) He, Y.; Lutz, T. R.; Ediger, M. D. *Macromolecules* **2003**, *36*, 8040−8048.
(27) Bovey, F. A.; Mirau, P. A. *NMR of Polymers*; Academic Press: San Diego, 1996.
(28) Abragam, A. *The Principle of Nuclear Magnetism*; Clarendon Press: Oxford, 1961; Chaper VIII.
(29) Heatley, F. *Annu. Rep. NMR Spectrosc.* **1986**, *17*, 179−230 and references therein.
(30) Heatley, F. *Prog. Nucl. Magn. Reson. Spectrosc.* **1979**, *13*, 47−85 and references therein.
(31) Loewenstein, A. *Advances in Nuclear Quadrupole Resonance*; John Wiley & Sons: London, 1983; Vol. 5.
(32) Lucken, E. A. C. *Nuclear Quadrupole Coupling Constants*; Academic Press: London, 1969.
(33) Bandis, A.; Wen, W. Y.; Jones, E. B.; Kaskan, P.; Jones, A. A.; Inglefield, P. T.; Bendler, J. T. *J. Polym. Sci., Polym. Phys. Ed.* **1994**, *32*, 1707−1717.
(34) Moe, N. E.; Qiu, X. H.; Ediger, M. D. *Macromolecules* **2000**, *33*, 2145−2152.
(35) Qiu, X. H.; Moe, N. E.; Ediger, M. D.; Fetters, L. J. *J. Chem. Phys.* **2000**, *113*, 2918−2926.
(36) Williams, M. L.; Landel, R. F.; Ferry, J. D. *J. Am. Chem. Soc.* **1955**, *77*, 3701−3707.
(37) Tammann, G.; Hesse, W. *Z. Anorg. Allg. Chem.* **1926**, *156*, 245.
(38) Moritani, T.; Fujiwara, Y. *J. Chem. Phys.* **1973**, *59*, 1175−1189.
(39) Ayyagari, C.; Bedrov, D.; Smith, G. D. *Macromolecules* **2000**, *33*, 6194−6199.
(40) vanGunsteren, W. F.; Berendsen, H. J. C. *Mol. Phys.* **1982**, *45*, 637−647.
(41) Cho, J.; Sanchez, I. C. PVT Relationships and Equations of State of Polymers. In *Polymer Handbook*, 4th ed.; Brandrup, J., Immergut, E. H.,Grulke, E. A., Eds.; Wiley-Interscience: New York, 1999.
(42) Ryckaert, J.; Ciccotti, G.; Berendsen, H. J. C. *J. Comput. Phys.* **1977**, *23*, 327−341.
(43) Darden, T.; York, D.; Pedersen, L. *J. Chem. Phys.* **1993**, *98*, 10089−10092.
(44) Martyna, G. J.; Tuckerman, M. E.; Tobias, D. J.; Klein, M. L. *Mol. Phys.* **1996**, *87*, 1117−1157.
(45) Laupretre, F.; Monnerie, L.; Roovers, *J. PMSE Prepr.* **2000**, *82*, 154.
(46) Santangelo, P. G.; Roland, C. M. *Macromolecules* **1998**, *31*, 4581−4585.
(47) Roland, C. M.; Ngai, K. L.; Santangelo, P. G.; Qiu, X. H.; Ediger, M. D.; Plazek, D. J. *Macromolecules* **2001**, *34*, 6159−6160.
(48) Plazek, D. J. *J. Phys. Chem.* **1965**, *69*, 3480−3487.
(49) Ngai, K. L.; Plazek, D. J. *J. Polym. Sci., Polym. Phys. Ed.* **1986**, *24*, 619−632.
(50) Chapman, B. R.; Hamersky, M. W.; Milhaupt, J. M.; Kostelecky, C.; Lodge, T. P.; von Meerwall, E. D.; Smith, S. D. *Macromolecules* **1998**, *31*, 4562−4573.
(51) Urakawa, O.; Swallen, S. F.; Ediger, M. D.; Von Meerwall, E. D. *Macromolecules* **2004**, *37*, 1558−1564.
(52) Pschorn, U.; Rossler, E.; Sillescu, H.; Kaufmann, S.; Schaefer, D.; Spiess, H. W. *Macromolecules* **1991**, *24*, 398−402.
(53) Rossler, E. Dissertation, University of Mainz, 1984.
(54) Pschorn, U. Dissertation, University of Mainz, 1985.
(55) Wefing, S.; Kaufmann, S.; Spiess, H. W. J. *J. Chem. Phys.* **1988**, *89*, 1234−1244.
(56) Kaufmann, S.; Wefing, S.; Schaefer, D.; Spiess, H. W. *J. Chem. Phys.* **1990**, *93*, 197−214.
(57) Spiess, H. W.; Sillescu, H. *J. Magn. Reson.* **1981**, *42*, 381−389.

MA049843R